The second-order spin-wave instability threshold in single-crystal yttrium-iron-garnet films under perpendicular pumping

Y. T. Zhang,[a] C. E. Patton, and G. Srinivasan
Department of Physics, Colorado State University, Fort Collins, Colorado 80523

(Received 16 October 1987; accepted for publication 3 February 1988)

The second-order spin-wave instability threshold in yttrium-iron-garnet single-crystal thin films has been investigated under conditions of ferromagnetic resonance (FMR). The samples were (111) etched circular films of 500 μm diam and 5.1 μm thickness, grown on gadolinium gallium garnet substrates by liquid-phase epitaxy. The pulsed microwave power FMR absorption curves were measured by standard signal averaging techniques at 9.18 GHz and room temperature for three different perpendicular pumping configurations: (1) in-plane static field and out-of-plane microwave field, (2) mutually perpendicular in-plane static and microwave fields, and (3) out-of-plane static field and in-plane microwave field. The experimental results show that the upsweep and downsweep FMR curves for lower pulsed microwave powers at low duty cycle of 1% are identical, but there are foldover effects in the FMR profiles at higher powers. Theoretical expressions for the instability threshold for these three configurations were obtained by extending previous theories. The calculated thresholds are in good agreement with the experimental results for configurations (1) and (2). The results for configuration (3) indicate the presence of a true foldover effect, also consistent with instability theory.

I. INTRODUCTION

There has been renewed attention to foldover effects and ferromagnetic resonance (FMR) saturation phenomena in single-crystal ferrites in recent years,[1,2] motivated in part by (a) the availability of high-quality epitaxial thin films of yttrium iron garnet (YIG), (b) potential magnetic film device applications at microwave and millimeter wave frequencies, and (c) the opportunity for a better understanding of the nonlinear and relaxation processes in ferrite materials. The present study has been preceeded by work on bulk single crystals of hexagonal ferrite[3,4] and YIG.[5] The basic high-power effect in all of these investigations was the appearance of an extended resonance when sweeping the static field in one direction and a sharp cusp when sweeping in the other. A typical set of "upsweep" and "downsweep" FMR absorption curve profiles from Ref. 2 is shown in Fig. 1, for the cw excitation of FMR in a YIG single-crystal film.

It was initially believed that these effects were connected with a foldover of the FMR profile which was related to the nonlinear magnetization dynamics in the materials. However, detailed profile measurements under pulsed microwave excitation conditions showed that the "foldover" characteristics disappeared under low duty cycle conditions, at least for the YIG film materials.[2] The only effect of the higher power excitation on the low duty cycle FMR profiles was a gradual broadening of the absorption peak, reminiscent of the resonance saturation effects in ferrites first observed by Damon[6] and Bloembergen and Wang[7] and later explained by Suhl in terms of instability processes.[8] A simple modification of the Suhl threshold formula was found to give a reasonable correlation between the observed threshold field for low duty cycle FMR saturation and theory.

The purpose of this work was to further test the hypothesis that the high-power broadening of the FMR in YIG

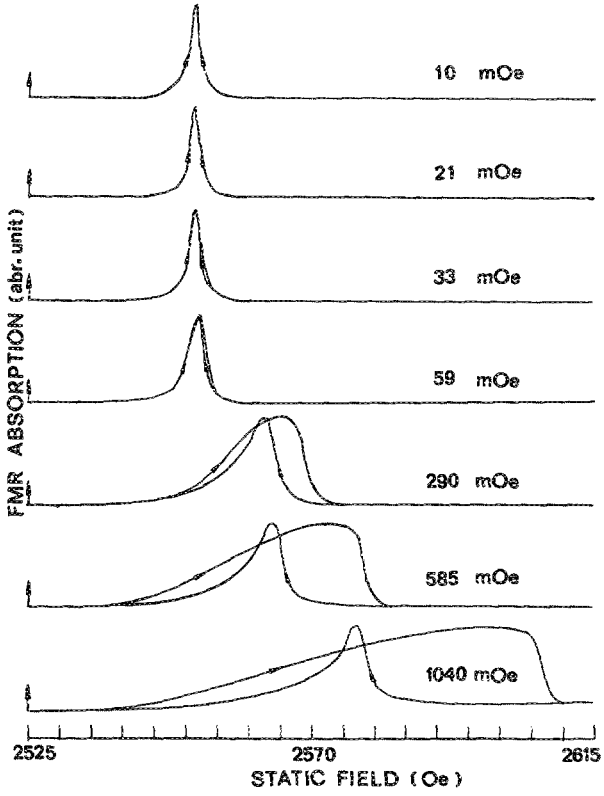

FIG. 1. Upsweep and downsweep FMR curves for different incident cw power levels and for a single-crystal YIG film at room temperature and 9.18 GHz, from Ref. 2. The number given for each set of curves indicates the microwave field amplitude at the sample position in mOe. The sweep rate was 40 Oe/min.

[a] Y. T. Zhang was a visiting scholar from the Shanghai University of Science and Technology, Shanghai, People's Republic of China from May 1985 through April 1987.

 0021-8979/88/115433-06$02.40 © 1988 American Institute of Physics

Downloaded 26 Dec 2001 to 129.82.140.114. Redistribution subject to AIP license or copyright, see http://ojps.aip.org/japo/japcr.jsp

films under low duty cycle conditions is due to spin-wave instability processes. This was done by obtaining low duty cycle FMR profiles similar to those in Ref. 2, but for three different static field microwave field orientation combinations: (1) in-plane static field and out-of-plane microwave field, (2) mutually perpendicular in-plane static and microwave fields, and (3) out-of-plane static field and in-plane microwave field. One would expect the coupling between the microwave pump field and the FMR mode to be weaker for case (1) than case (2), for example. The corresponding Suhl threshold power for FMR saturation would be higher. Case (3) corresponds to a circular polarization for the FMR response and geometric conditions in which classical foldover[9] might actually be observed. The basic strategy, then, was to measure the FMR profiles and determine resonance saturation threshold field values for the three different configurations and compare the results with predictions from theory.

It is found that the threshold for FMR saturation when the static field is in-plane is indeed higher for an out-of-plane microwave pump than for an in-plane pump. The experimental thresholds for these two situations, 31 and 23 mOe, are reasonably consistent with theoretical values. Moreover, the out-of-plane static field situation gives rise to a low field shoulder in the FMR profile, even under low duty cycle conditions, which is consistent with geometric foldover.

II. EXPERIMENT AND RESULTS

These experiments were carried out using a modified Varian Model 4500 microwave spectrometer at 9.18 GHz and room temperature. The experimental system is shown schematically in Fig. 2. A single-crystal (111) YIG film, 5.1 μm in thickness and etched to produce a 500-μm-diam circle, was used in these experiments. The sample had an FMR linewidth of 2.0 Oe in the in-plane static field cases and 1.7 Oe for the out-of-plane case. The sample was mounted on a low loss dielectric rod at the center of a critically coupled reflected TE_{102} cavity with a loaded Q of about 2500. This Q was measured by the method described in Ref. 10. The reflected microwave power from cavity was monitored with a conventional diode detector. Precision attenuator A controls the microwave power incident on the sample. The maximum peak power was 300 mW, corresponding to a microwave field amplitude of 1040 mOe at the sample position. Precision attenuator B was used in such a way that all FMR absorption curves could be obtained with approximately the same power at the detector. A p-i-n diode switch was used to obtain pulsed microwave power with different pulse widths (10 μs–10 ms) and duty cycles (1%–100%). As demonstrated in Ref. 2, the second-order spin-wave instability threshold for narrow linewidth YIG can be determined from measured FMR profiles for increasing microwave pulsed power levels only by using pulse power at low duty cycles. The FMR absorption profiles discussed below were obtained by this procedure. All FMR curves were observed by sweeping the applied static field at a fixed rate of 40 Oe/min.

In order to determine experimental thresholds for configurations (1) and (2), FMR absorption profiles were first obtained for a sequence of increasing power levels. Plots of inverse half-power linewidth versus inverse microwave field amplitude were then used to obtain threshold values. The series of profiles for configuration (1), an out-of-plane microwave field and an in-plane static field, is shown in Fig. 3.

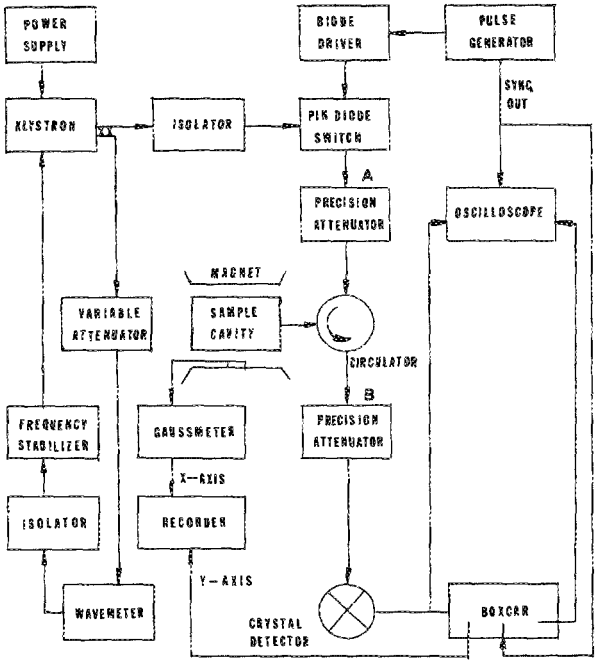

FIG. 2. Schematic diagram of the experimental apparatus used to measure the pulsed power FMR absorption curves.

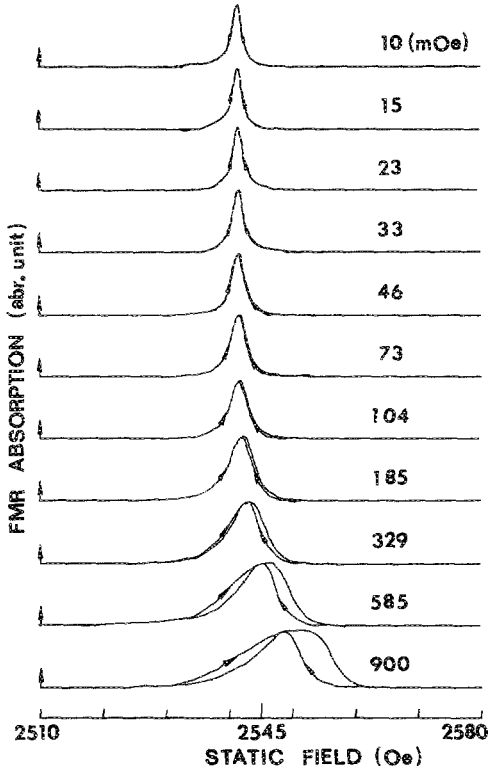

FIG. 3. Upsweep and downsweep FMR absorption curves for different values of the peak microwave power incident on the single-crystal YIG film, for a fixed duty cycle of 1% under perpendicular pumping with an in-plane static field and out-of-plane microwave field, corresponding to configuration (1). The number given for each set of curves indicates the microwave field amplitude at the sample position in mOe.

Downloaded 26 Dec 2001 to 129.82.140.114. Redistribution subject to AIP license or copyright, see http://ojps.aip.org/japo/japcr.jsp

The corresponding series for configuration (2), with the microwave and static fields both in-plane, is shown in Fig. 4. In both figures the power at the sample position for each pair of FMR traces, upsweep and downsweep static field, is given in terms of the linearly polarized microwave field amplitude at the sample position in mOe. The microwave excitation consisted of 100-μs pulses at a 1% duty cycle, as in Ref. 2.

Both figures show the essential effect described earlier, a gradual broadening of the FMR profile as the power level is increased. (The shifts and hysteresis at the highest powers will be discussed shortly.) The broadening has been quantitatively analyzed by examining the variation in inverse linewidth with inverse microwave field amplitude. Such plots are shown in Fig. 5(a) for configuration (1) and in Fig. 5(b) for configuration (2). Extrapolations of the linear portions of the data at high power (low inverse field amplitude) to the "baseline" at $1/\Delta H = 0.5$ Oe^{-1} yield threshold field values (h_{crit}) of 31 and 23 mOe, respectively, for the two configurations. These values will be compared with theoretical threshold estimates in the next section. It is important to point out that the onset of saturation is rather gradual in both cases and the assignment of discrete threshold values is somewhat arbitrary. The trend of the data is still clear. The onset does occur at a higher microwave power level for configuration (1) than for configuration (2).

The traces at the highest powers in Figs. 3 and 4 do show shifts to higher fields, the development of high field shoulders, asymmetric profiles, and hysteresis. These effects are

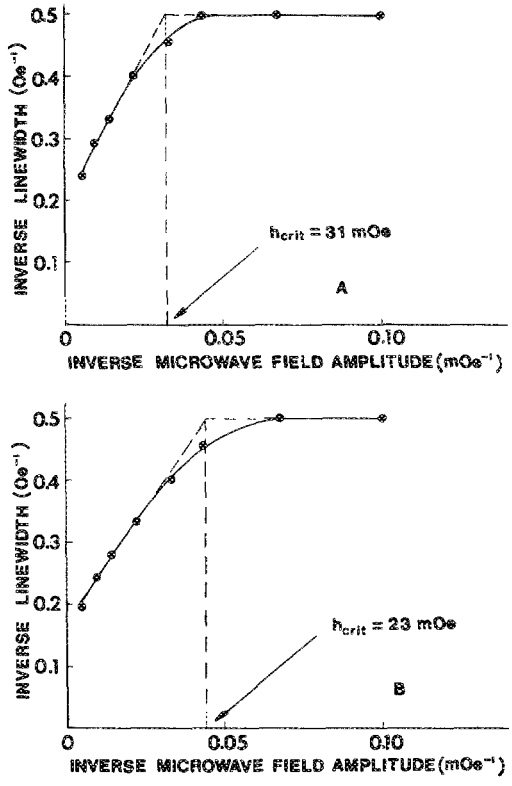

FIG. 5. Inverse linewidth vs inverse microwave field amplitude for (a) configuration (1) and (b) configuration (2), as obtained from the data of Figs. 3 and 4, respectively.

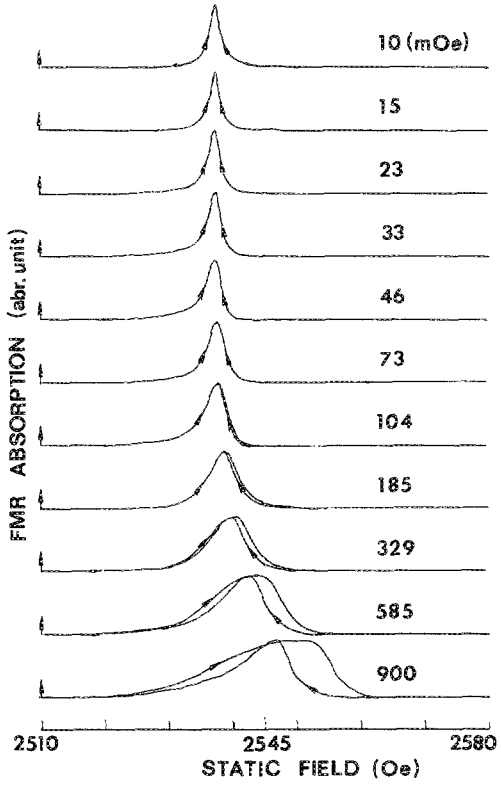

FIG. 4. Upsweep and downsweep FMR absorption curves for different values of the peak microwave power incident on the single-crystal YIG film, for a fixed duty cycle of 1% under perpendicular pumping. The mutually perpendicular static and microwave fields are both in-plane, corresponding to configuration (2). The number given for each set of curves indicates the microwave field amplitude at the sample position in mOe.

probably related to a decrease in the effective static magnetization from one or more of the following: (1) The spin-wave instability processes in themselves lead to a reduction in the effective M_s because of the generation of nonzero wavevector parametric spin waves. (2) A large precession cone angle reduces the effective M_s. (3) Some residual heating at the highest powers, even for a low duty cycle, can reduce M_s. We will return to these and related effects shortly.

The corresponding FMR profiles for configuration (3), for which the static field is perpendicular to the film plane, are shown in Fig. 6. As before, microwave field amplitudes for each pair of FMR traces are indicated. The results for configuration (3) are rather different from those shown in Figs. 3 and 4. Here, increasing power results in a distinct shoulder on the low field side of the FMR trace. Up to a microwave field amplitude of about 200 mOe this shoulder has *no* hysteresis. That is, the upsweep and downsweep traces are identical. The traces for the three highest powers show extended shoulders for both upsweep and downsweep conditions. It is to be emphasized that these curves are for a 1% pulse microwave duty cycle. The shoulder hysteresis behavior is quite different from the shoulder cusp characteristics in Fig. 1 attributed to heating.

It is noteworthy that the shoulder development for configuration (3) occurs on the low field side of the FMR line, in contrast to the high field shoulder development for the highest power traces for configurations (1) and (2). The directionality in these different situations is consistent with a reduction in the effective static magnetization. Configura-

Downloaded 26 Dec 2001 to 129.82.140.114. Redistribution subject to AIP license or copyright, see http://ojps.aip.org/japo/japcr.jsp

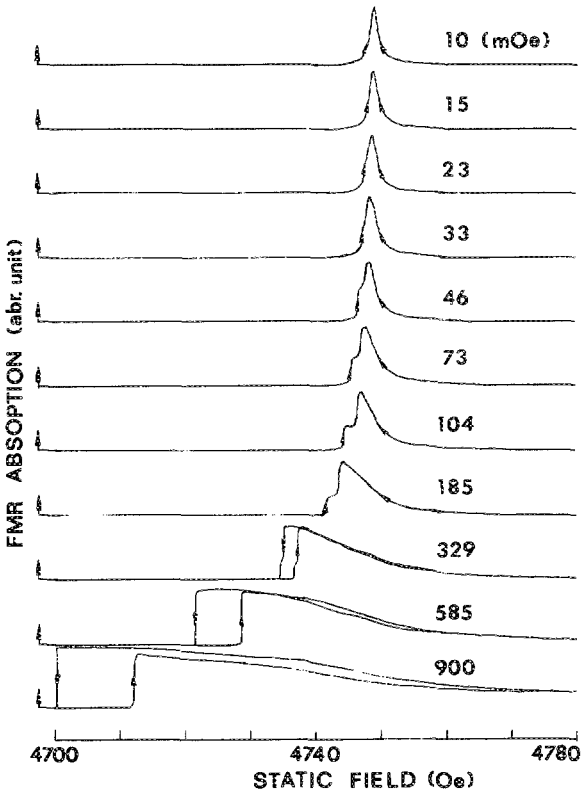

FIG. 6. Upsweep and downsweep FMR absorption curves for different values of the peak microwave power incident on the single-crystal YIG film, for a fixed duty cycle of 1% under perpendicular pumping. The static field was out-of-plane and the microwave field was in-plane, corresponding to configuration (3). The number given for each set of curves indicates the microwave field amplitude at the sample position in mOe.

tions (1) and (2) are for an in-plane static field and an FMR condition given by

$$\omega = \gamma[H(H + 4\pi M_s)]^{1/2} . \tag{1}$$

Configuration (3) corresponds to an FMR condition given by

$$\omega = \gamma(H - 4\pi M_s) . \tag{2}$$

In both of the FMR equations given above, γ denotes the gyromagnetic ratio, $4\pi M_s$ is the saturation induction, H is the static applied field, and ω is the FMR frequency. For configurations (1) and (2), it is clear that a decrease in $4\pi M_s$ will result in an *increase* in the field for FMR at fixed ω. For configuration (3), a drop in $4\pi M_s$ causes the FMR field to *decrease*. As already mentioned, several factors could lead to a reduction in the effective $4\pi M_s$ value. We will return to a brief discussion of these effects for configuration (3) at the end of the next section.

III. ANALYSIS AND DISCUSSION

Suhl[8] first developed the theory of spin-wave instability processes for FMR in ferrites. A related theory for parallel pumping, with the microwave field parallel to the static field, was developed by Schlömann, Green, and Milano.[11] These theories were later extended to include pumping with a general microwave field polarization and a general ellipsoid sample shape.[12] Reference 12 presented specific formulas for first-order spin-wave instability thresholds, expressed in terms of a coupling coefficient $G_k^{(1)}$ for the specific parametric spin-wave modes driven by the microwave pump. The terminology "first order" refers to the subset of terms in the working equations which lead to instability. Only terms which contained a single amplitude factor α_0 for the FMR uniform precession mode were considered.

Following the procedure of Ref. 12, one may construct expressions from the second-order terms in the theory, that is, those terms in G_k which contain products of α_0 factors, and derive equations for the second-order spin-wave instability threshold under conditions of a general pumping polarization and a general ellipsoid sample shape. That procedure has been followed to obtain threshold expressions for the three configurations of interest here. Magnetocrystalline anisotropy effects were not considered. The basic working equations, following the terminology of Ref. 12, are given in the Appendix. The reader should consult Ref. 12 for a detailed discussion of the theoretical framework and operational parameters. The pertinent threshold expressions are given below:

$$h_{\text{crit}}^{(\text{Config.1})} = \Delta H \frac{(2\gamma H + \omega_m)}{(\omega + \gamma H)} \left(\frac{\gamma \Delta H_k}{(\omega_m - \gamma H + \omega)} \right)^{1/2} , \tag{3}$$

$$h_{\text{crit}}^{(\text{Config.2})} = \Delta H \frac{(2\gamma H + \omega_m)}{(\omega + \omega_m + \gamma H)} \left(\frac{\gamma \Delta H_k}{(\omega_m - \gamma H + \omega)} \right)^{1/2} , \tag{4}$$

$$h_{\text{crit}}^{(\text{Config.3})} = \Delta H \left(\frac{\gamma \Delta H_k}{\omega_m} \right)^{1/2} . \tag{5}$$

In Eqs. (3)–(5), ΔH denotes the half-power FMR linewidth, ΔH_k is the spin-wave linewidth, and $\omega_m = \gamma 4\pi M_s$ expresses the saturation induction $4\pi M_s$ in frequency units. The low-power FMR frequency ω is connected to H, γ, and $4\pi M_s$ through the appropriate FMR equation, Eq. (1) for in-plane H and Eq. (2) for out-of-plane H. The ΔH_k parameter is not an actual linewidth; it simply expresses the spin-wave relaxation rate η_k in linewidth units, according to $\Delta H_k = 2\eta_k/\gamma$.

The above equations differ from the standard formulas in the early references on resonance saturation in that *both* ΔH and ΔH_k linewidth parameters appear. The FMR linewidth ΔH is related to the uniform mode amplitude, while the spin-wave linewidth ΔH_k is related to the relaxation of energy from the spin-wave mode which goes unstable. These linewidths may be (and usually are) different, even in single crystals.

Equations (3) and (4) have been used to obtain theoretical threshold values for configurations (1) and (2), respectively. Assuming a spin-wave linewidth ΔH_k parameter of 0.5 Oe (typical for single-crystal YIG) and an FMR linewidth of 2 Oe (the measured low-power linewidth for the in-plane static field cases), one obtains theoretical h_{crit} values of 34 and 27 mOe for configurations (1) and (2), respectively. Typical γ and $4\pi M_s$ values of 1.76×10^7 $\text{Oe}^{-1}\,\text{s}^{-1}$ and 1750 G were used for these evaluations. These thresholds are in reasonable agreement with the experimental values of 31 and 23 mOe from Fig. 5. Considering the gradual

Downloaded 26 Dec 2001 to 129.82.140.114. Redistribution subject to AIP license or copyright, see http://ojps.aip.org/japo/japcr.jsp

nature of the actual onset of the instability in Fig. 5 and the leeway in choosing the ΔH_k parameter in the theory, this agreement may be considered to be excellent. The primary physical significance here lies in the agreement between the *relative* thresholds. The h_{crit} values are higher by some 25%–30% for configuration (1) compared to configuration (2), for both the experiment and the theory.

Configuration (3) presents a problematic situation for h_{crit} comparisons, since the developing low field shoulders complicate any extrapolation of the linebroadening data to determine experimental threshold values. The calculated threshold from Eq. (5), based on the YIG parameters given above and an FMR linewidth of 1.7 Oe (as measured in the perpendicular case), is 29 mOe. An extrapolation of the sort shown in Fig. 5 for the profiles in Fig. 6 yields an h_{crit} value of 23 mOe. The distortions which are present in the case of configuration (3) lead to an experimental threshold extrapolation which is somewhat lower (but marginally so) than one would expect from the other results.

The significance of the high field shoulder development at the highest powers for configurations (1) and (2) and the more pronounced low field shoulders for configuration (3) was briefly discussed in the previous section. The perpendicular static field case, configuration (3), shows distinct shoulders with a well-defined hysteresis. That is, the shoulder displacement from the low-power FMR position for a downsweep or decreasing field is *larger* than the corresponding displacement for an upsweep (increasing) field. Foldover effects for this configuration have been treated in detail by Schlömann.[13]

As discussed above, the basic shoulder effect is due to a reduction in the effective $4\pi M_s$ value at high power. However, if one considers only the linear FMR response at high power and ignores the nonlinear spin-wave effects, the predicted reduction in $4\pi M_s$ [and hence the downshift in FMR position from Eq. (2)] is hundreds of Oe, rather than the tens of Oe found experimentally. Schlömann, in calculating the response above threshold, showed that the instability processes which give rise to h_{crit} effects also serve to limit the FMR precession cone amplitude above threshold. He also showed that the FMR absorption profile can become rather distorted and take on a peculiar "folded-over" character at high-power levels. The basic effect is that the FMR amplitude ceases to continue to increase with microwave power when the microwave field amplitude exceeds h_{crit}. The observed decline in the susceptibility at resonance under high-power conditions is one well-known effect of this h_{crit} process. This reduced FMR response above threshold, in turn, leads to a reduced downshift in field in the FMR position. The net effect is a reduced shift of tens of Oe rather than the hundreds of Oe expected from the linear theory. Estimates of the expected shifts from the equations in Ref. 13 show a factor of 2 agreement with the data for configuration (3), with a calculated FMR peak shift of about 25 Oe for a microwave pump field of 900 mOe. The corresponding bottom set of traces in Fig. 6 shows downsweep and upsweep shoulder position shifts of about 50 and 40 Oe, respectively, relative to low-power FMR. Foldover effects will be discussed in detail in a separate publication.

ACKNOWLEDGMENT

The authors gratefully acknowledge Dr. J. D. Adam, Westinghouse Research Laboratory, Pittsburgh, PA, for the single-crystal YIG films which were used in this study.

APPENDIX

Reference 12 describes a general theory for so-called "first-order" spin-wave instability processes. The purpose of this Appendix is to summarize the important working equations to apply the theory to "second-order" processes and obtain the h_{crit} expressions given in Sec. III.

The basic approach is to expand the undamped equation of motion for the vector magnetization, $\mathbf{M}(\mathbf{r}) = M_s \boldsymbol{\alpha}(\mathbf{r})$, in a Fourier series,

$$\boldsymbol{\alpha}(\mathbf{r}) = \sum_k \boldsymbol{\alpha}_k e^{i\mathbf{k}\cdot\mathbf{r}} , \tag{A1}$$

and obtain a equation of motion for the spin-wave amplitudes [the α_k in Eq. (A1)] which involves the microwave field $\mathbf{h}$ and the uniform precession (or FMR) amplitude α_0. Under certain conditions, it is possible to obtain solutions for the spin-wave amplitudes which grow exponentially with time. The unstable growth occurs when the microwave field amplitude exceeds some threshold value, h_{crit}.

The formulation is described in detail in Ref. 12. Specific results are given for "first-order" processes which involve the instability of spin waves at *one-half* the microwave pump frequency. The threshold field is obtained by equating the coefficient for the energy flow into a particular spin-wave mode, $G_k^{(1)}$, and the relaxation rate η_k. The label "first order" comes from the fact that $G_k^{(1)}$ involves only first-order terms in the complex uniform mode amplitude α_0 and microwave field $\mathbf{h}$. Reference 12 presents specific equations for $G_k^{(1)}$ and particular applications of the first-order theory.

For FMR in YIG materials at x-band frequencies, there are no half-frequency spin waves available to couple energy from the uniform precession mode. It is necessary to consider "second-order" instability processes. These processes involve spin waves *at* the pump frequency, $\omega_k = \omega$. The corresponding $G_k^{(2)}$ coupling term contains second-order products of α_0 and $\mathbf{h}$ terms. Following the nomenclature of Ref. 12, one may write the general expression for $G_k^{(2)}$ as

$$G_k^{(2)} = (\gamma h_0/2)^2 \left[e^{+2i\phi_k}/(4\omega) \right] W^{(2)} , \tag{A2}$$

where $W^{(2)}$ is given by

$$W^{(2)} = (A_k + \omega)(\sigma q_L^2 + q_L) e^{-2i\phi_k} + (A_k - \omega)(\sigma q_A^2 + q_A^*) e^{+2i\phi_k} - B_k (q_L + q_A^*) . \tag{A3}$$

The σ parameter in Eq. (A3) is given by

$$\sigma = \gamma (Dk^2 + 4\pi M_s \cos^2 \theta_k) . \tag{A4}$$

In the above, θ_k and ϕ_k denote the polar and aximuthal spin-wave propagation angles for a spin wave of wave vector $\mathbf{k}$ (wave number k) and frequency $\omega_k = \omega$; h_0 is the amplitude of the linearly polarized microwave pump field at ω. The D parameter in Eq. (A4) is the usual phenomenological exchange coefficient which occurs in the spin-wave dispersion equation,

Downloaded 26 Dec 2001 to 129.82.140.114. Redistribution subject to AIP license or copyright, see http://ojps.aip.org/japo/japcr.jsp

$$\omega_k = \gamma[(H_i + Dk^2)(H_i + Dk^2 + 4\pi M_s \sin^2\theta_k)]^{1/2}, \tag{A5}$$

where H_i is the static *internal* field. A_k and B_k are the usual parameters encountered in the spin-wave theory:

$$A_k = \gamma(H_i + Dk^2 + 2\pi M_s \sin^2\theta_k), \tag{A6a}$$

$$B_k = \gamma 2\pi M_s \sin^2\theta_k, \tag{A6b}$$

$$\omega_k = (A_k^2 - B_k^2)^{1/2}. \tag{A7}$$

q_L and q_A in Eq. (A3) are reduced expressions for the Larmor and anti-Larmor circularly polarized components of the uniform precession response.

To evaluate the h_{crit} threshold, it is necessary to consider only the solutions to $|G_k^{(2)}| = \eta_k$ which yield the *smallest* threshold. For second-order processes at resonance, this minimum threshold occurs for $\theta_k = 0$. One may ignore the anti-Larmor q_A terms in $G_k^{(2)}$ at resonance. The Larmor response $|q_L|$ at resonance is given by the following expressions:

Configuration (1):

$$|q_L| = [2(\omega/\gamma + H)]/[\gamma\Delta H(2H + 4\pi M_s)]. \tag{A8}$$

Configuration (2):

$$|q_L| = [2(\omega/\gamma + H + 4\pi M_s)]/[\gamma\Delta H(2H + 4\pi M_s)]. \tag{A9}$$

Configuration (3):

$$|q_L| = 2/(\gamma\Delta H). \tag{A10}$$

These q_L expressions differ from those in Ref. 12 in several respects. First, the expressions are explicitly for a frequency ω and static applied field H which satisfy the appropriate FMR configuration, Eq. (1) for configurations (1) and (2), and Eq. (2) for configuration (3). Second, the $|q_L|$ equations include the effect of damping, as evident from the ΔH terms in the denominators. Note that the $|q_L|$ for configuration (2) is clearly larger than the $|q_L|$ for configuration (1). This is related to the more efficient coupling of the in-plane microwave field to the uniform precession mode for configuration (2). The uniform mode response equations in Ref. 12 were developed for subsidiary absorption and parallel pumping at fields well below the FMR position, such that the damping could be neglected. Finally, the present $|q_L|$ expressions are for the the specific microwave/static field/thin-film configurations indicated, not for a general polarization and ellipsoidal sample.

Returning now to the threshold condition $|G_k^{(2)}| = \eta_k$, we note that the condition $\theta_k = 0$, the neglect of anti-Larmor q_A and q_A^* terms, and the condition $\sigma q_L \gg 1$ greatly simplify Eq. (A2). This simplified threshold condition is given by

$$|G_k^{(2)}| = (\gamma h_0/2)^2(\sigma q_L^2/2) = \gamma\Delta H_k/2. \tag{A11}$$

In Eq. (A11), we have also used the fact that $A_k = \omega$ is satisfied for $\theta_k = 0$. The σ parameter may also be written as

$$\sigma = \omega - \gamma H_i + 4\pi M_s \tag{A12}$$

for $\theta_k = 0$. Recall that H_i is the *internal* static field [H for configurations (1) and (2), and $H - 4\pi M_s$ for configuration (3)].

The above working equations combine to produce the threshold field h_{crit} expressions given by Eqs. (3)–(5) when Eq. (A11) is solved for h_0, based on the $|q_L|$ expressions in Eqs. (A8)–(A10).

[1] J. Seagle, S. H. Charap, and J. O. Artman, J. Appl. Phys. **57**, 3706 (1985).
[2] Y. T. Zhang, C. E. Patton, and M. V. Kogekar, IEEE Trans. Mag. **22**, 993 (1986).
[3] I. B. Goldberg, J. Appl. Phys. **51**, 1857 (1980).
[4] L. M. Silber, C. E. Patton, and H. V. Naqvi, J. Appl. Phys. **54**, 4071 (1983).
[5] K. D. McKinstry, C. E. Patton, and M. V. Kogekar, J. Appl. Phys. **58**, 925 (1985).
[6] R. W. Damon, Rev. Mode. Phys. **25**, 239 (1953).
[7] N. Bloembergen and S. Wang, Phys. Rev. **93**, 72 (1954).
[8] H. Suhl, J. Phys. Chem. Solids **1**, 209 (1957).
[9] P. W. Anderson and H. Suhl, Phys. Rev. **100**, 1788 (1955).
[10] Z. Frait and C. E. Patton, Rev. Sci. Instrum. **51**, 1092 (1980).
[11] E. Schlömann, J. J. Green, and U. Milano, J. Appl. Phys. **31**, 3865 (1960).
[12] C. E. Patton, J. Appl. Phys. **40**, 2837 (1969).
[13] E. Schlömann, Raytheon Tech. Rep. No. R-48 (1959) (unpublished).

Downloaded 26 Dec 2001 to 129.82.140.114. Redistribution subject to AIP license or copyright, see http://ojps.aip.org/japo/japcr.jsp